

Gravitational waves as a probe of dark matter mini-spikes

Kazunari Eda,^{1,2,*} Yousuke Itoh,² Sachiko Kuroyanagi,³ and Joseph Silk^{4,5,6}

¹ *Department of Physics, Graduate School of Science,
The University of Tokyo, Tokyo, 113-0033, Japan*

² *Research center for the early universe (RESCEU),
Graduate School of Science, The University of Tokyo, Tokyo, 113-0033, Japan*

³ *Department of Physics, Faculty of Science, Tokyo University of Science,
1-3, Kagurazaka, Shinjuku-ku, Tokyo 162-8601, Japan*

⁴ *Institut d' Astrophysique, UMR 7095, CNRS,
UPMC Univ. Paris VI, 98 bis Boulevard Arago, Paris 75014, France*

⁵ *Department of Physics and Astronomy, The Johns Hopkins University, Baltimore, MD 21218, USA*

⁶ *Beecroft Institute for Particle Astrophysics and Cosmology,
Department of Physics, University of Oxford, Keble Road, Oxford, OX1 3RH, UK*

Recent studies show that an intermediate mass black hole (IMBH) may develop a dark matter (DM) mini-halo according to some BH formation scenarios. We consider a binary system composed of an IMBH surrounded by a DM mini-spike and a stellar mass object orbiting around the IMBH. The binary evolves due to gravitational pull and dynamical friction from the DM mini-spike and back-reaction from its gravitational wave (GW) radiation which can be detected by future space-borne GW experiments such as eLISA/NGO. We consider a single power-law model for the DM mini-spike which is assumed to consist of non-annihilating DM particles and demonstrate that an eLISA/NGO detection of GW from such a binary enables us to measure the DM mini-spike parameters very accurately. For instance, in our reference case originally advocated by Zhao and Silk (2005) and Bertone et al. (2005), we could determine the power-law index α of the DM mini-spike radial profile with a 1σ relative error of $\pm 5 \times 10^{-6}$ for a GW signal with signal-to-noise-ratio 10 and assuming a 5 year observation with eLISA. We also investigate how accurately the DM parameters can be determined for various DM parameters and the masses of the IMBH-stellar mass object binary surrounded by a DM mini-spike. We find that we can determine the power-law index α at 10 % level even for a slightly flatter radial distribution of $\alpha \sim 1.7$.

I. INTRODUCTION

There is much reliable evidence for the existence of dark matter (DM) which is mainly associated with the missing mass problem. Astronomers and particle physicists seek to probe DM properties by direct laboratory experiments or indirect observations [3]. Indirect techniques include efforts to detect gamma rays from DM annihilation using telescopes such as the Fermi Large Area Telescope (Fermi-LAT, [4]), the Major Atmospheric Gamma-ray Imaging Cherenkov (MAGIC) telescope [5], the High Energy Stereoscopic System (H.E.S.S., [6]) and the Very Energetic Radiation Imaging Telescope Array System (VERITAS, [7]) (see, e.g., [8] for a review).

It was first suggested by Gondolo and Silk [9] that adiabatic growth of a BH at the center of a DM halo whose density had a singular power-law cusp $\rho(r) \propto r^{-\alpha_{\text{ini}}}$ with $0 \leq \alpha_{\text{ini}} \leq 2$ led to a high density DM region around the central BH, $\rho_{\text{spike}}(r) \propto r^{-\alpha}$ with $2.25 \leq \alpha \leq 2.5$. This region is called a DM spike. Inside the spike, DM annihilations are enhanced and produce the strong gamma-ray photon flux which could be detectable to the telescopes mentioned above.

However, subsequent studies pointed out that this spike could be weakened by dynamical processes such as mergers of host-galaxies, sub-halo accretion and passing of molecular clouds [10–14]. These processes transfer energy to the DM particles and destroy the structure of the DM spike. Then the annihilation rate in the spike is smaller than predicted in [9] because it depends on the line-of-sight integral of the squared density of the spike. If supermassive black holes (SMBHs) have experienced mergers, they are unlikely to have surviving spike structure. Even this however is controversial because of the uncertainty in whether the final parsec problem for SMBH mergers has been resolved phenomenologically [15] or even theoretically [16]. On the other hand, formation scenarios of intermediate-mass black holes (IMBH) which allow DM mini-spikes have been proposed [1, 2]. If the IMBH have never experienced mergers in the past, the DM mini-spike around the central IMBH is likely to survive.

IMBHs may exist in our universe [17], and even several hundreds would reside in the halo of the present-day Milky Way galaxy [18, 19]. Those IMBHs in globular clusters are recognized as promising sources for the evolved

*Electronic address: eda@resceu.s.u-tokyo.ac.jp

Laser Interferometer Space Antenna (eLISA) [20] / the New Gravitational Wave Observatory (NGO) [21] and DECi-hertz Interferometer Gravitational Wave Observatory (DECIGO)[22].

In our previous work [23], we demonstrated that a very tiny effect such as the gravitational pull of a DM mini-spike around an IMBH indeed affects detectability of GW by eLISA and thereby we could infer presence or absence of a DM mini-spike around an IMBH using GW. Specifically, when a stellar mass object inspirals into the central IMBH, it is affected by the gravitational force of not only the central IMBH but also the mini-spike. Therefore the inspiral GW is modified by the mini-spike around the central IMBH. We found that the very tiny effect from gravitational pull of a DM mini-spike could have a large impact on detectability of the GW, thanks to the huge number of orbital cycles which the binary experienced in the eLISA detection frequency band. We also found that GW detectability strongly depends on the density profile of the DM mini-spike.

In this paper, we extend our previous work in the following way. We again consider GWs emitted from a binary system consisting of a stellar mass object and an IMBH harbored in a DM mini-spike, and calculate the GW waveform including the effect of both the gravitational potential and the dynamical friction on the falling stellar mass object in the DM mini-spike. Furthermore, we investigate how accurately the DM parameters are determined by the GW observations. We find that the DM information contained in the waveform can be extracted with very good accuracy by GW observations if the central IMBH has a steep density mini-spike. We also investigate how the detection accuracy of the DM parameters changes depending on the masses of the binary components and the density profile of the DM mini-spike such as the power index and overall normalization.

Recently Macedo et al. made clear the importance of the dynamical friction on the GW waveform in a quite different context from ours, namely, a stellar mass object falling in a compact configuration of DM clouds [24]. Also, Barausse et al. has given a wide survey on astrophysical environmental effects on GW signals using order of magnitude estimates, concluding that astrophysical environmental effects such as accretion disks, magnetic fields, and DM halos do not obscure gravitational wave astrophysics, e.g., precision measurements of binary masses and tests of general relativity [25] (See also [26]). To indicate one exception, our paper shall clearly show that, in the recently advocated DM mini-spike scenario, environmental effects do affect GW detectability [23] and we can measure DM properties quite accurately from eLISA GW detection, which will be shown through a detailed study using a matched filtering technique and Fisher matrix analysis.

We stress that while gamma-ray observations from DM annihilations can only work if the DM is a weakly interacting massive particle (WIMP), the GW observations we proposed should be widely applicable to any type of DM particles. Furthermore, matter is almost completely transparent to GWs unlike electromagnetic waves because of the smallness of their gravitational cross-section. Hence, the GWs carry pure information on the DM from the mini-spike to the detector. Future GW experiments will probe the structure of the DM mini-spike and will even offer a hint on the nature of the DM particle.

The rest of the paper is organized as follows. Sec. II presents the DM mini-spike model and candidates for the stellar mass object. In Sec. III we derive the GW waveform from the system which we consider and the observational errors of the waveform parameters are calculated in Sec. IV. Finally our conclusions are given in Sec. V.

II. MINI-HALO MODEL

A. Initial DM mini-halo profile

We assume that the initial DM mini-halo profile which leads to the DM mini-spike after the adiabatic growth of the IMBH is approximately described by the Navarro-Frenk-White (NFW) profile [27]

$$\rho_{\text{NFW}}(r) = \frac{\rho_s}{(r/r_s)(1+r/r_s)^2}, \quad (1)$$

where r is the radius, ρ is the mass density and the subscript ‘‘s’’ stands for the scaling. Navarro, Frenk and White obtained this profile via cosmological N-body numerical simulation and numerical fitting of obtained DM halo profiles around clusters of galaxies. Surprisingly, their simulations showed that every DM halo around a cluster of galaxies follows the NFW profile when normalized properly by ρ_s and r_s . Later work, however, shows that the inner slope may be slightly steeper than the NFW one ($\rho \propto r^{-1}$) and may not even be universal [28]. In any case, we refer to the NFW profile and the derived parameters listed in the table I below as our reference model in the following for simplicity. We study how accurately the dark matter parameters can be measured in our reference model in detail, then extend our analysis to different sets of values of the DM parameters to take into account ambiguities in the DM distribution around an IMBH.

The NFW parameters ρ_s and r_s are related to the cluster mass and concentration parameters by

$$M_{\text{vir}} = \frac{4\pi}{3} \Delta_{\text{vir}} \Omega_m(z_f) \rho_{\text{cri}}(z_f) r_{\text{vir}}^3, \quad (2a)$$

$$\rho_s \equiv \frac{1}{3f(c_{\text{vir}})} \Delta_{\text{vir}} \Omega_m(z_f) \rho_{\text{cri}}(z_f) c_{\text{vir}}^3, \quad (2b)$$

where $c_{\text{vir}} \equiv r_{\text{vir}}/r_s$ and r_{vir} is the virial radius and M_{vir} is the virial mass of the cluster, z_f is the formation redshift of the cluster, Ω_m is the matter density parameter, ρ_{cri} is the critical matter density of the universe and the function $f(x)$ is the volume integral of the NFW profile $f(x) \equiv \ln(1+x) - x/(1+x)$ (see, e.g., [29]). We used the fitting formula given by [30] for the parameter Δ_{vir} : $\Delta_{\text{vir}} \equiv 18\pi^2(1 + 0.4093\omega_{\text{vir}}^{0.9052})$ where $\omega_{\text{vir}} \equiv 1/\Omega_m(z_f) - 1$ [30]. The mass-concentration relation is taken from [31] which fits the profiles of the clusters of galaxies obtained in their N-body simulations. This result for clusters of galaxies may or may not apply for the mini-halo. In any case, concentration parameters between $O(1-1000)$ lead to qualitatively similar results and are given by the following relation.

$$c_{200} = A_{200} (M_{200}/M_{\text{pivot}})^{B_{200}} (1 + z_f)^{C_{200}}, \quad (3)$$

where we assume $(A_{200}, B_{200}, C_{200}, M_{\text{pivot}}) = (5.71, -0.084, -0.47, 1.0 \times 10^{14} h^{-1} M_{\odot})$ from the result of [31]. The parameters A_{200} and so on may be appropriately used when the overdensity Δ_{vir} equals 200. However, we here assumed $A_{200} \simeq A_{\text{vir}}$ and so on for simplicity.

As will be shown later, the GW waveform depends on the DM mini-spike slope α and some combination of the radius at which the mini-spike is established, r_{sp} , and the DM density there, ρ_{sp} . Under the assumption of adiabatic growth, while the final power-law index of the DM mini-spike, α , depends on the power-law index of the initial inner DM profile, the latter two depend on ρ_s , r_s and α . For concreteness, we adopt $M_{\text{vir}} = M_{\text{DM}} = 10^6 M_{\odot}$, $z_f = 20$ in Eqs. (2a), (2b), and (3) [1, 2] and find $c_{\text{vir}} = 6.6$, $r_s = 23.1 \text{pc}$, and $\rho_s = 3.8 \times 10^{-22} \text{g/cm}^3$.

B. DM mini-spike profile

We proceed to discuss the DM profile of the mini-spike. If the DM mini-halo initially has a cuspy profile $\rho(r) \propto r^{-\alpha_{\text{ini}}}$ with $0 \leq \alpha_{\text{ini}} \leq 2$, then the adiabatic growth of the central IMBH produces the DM mini-spike. Hence the dark matter profile becomes [9, 32]

$$\rho_{\text{DM}}(r) = \begin{cases} \rho_{\text{spike}}(r), & (r_{\text{min}} \leq r \leq r_{\text{sp}}), \\ \rho_{\text{NFW}}(r), & (r_{\text{sp}} < r), \end{cases} \quad (4)$$

with

$$\rho_{\text{spike}}(r) = \rho_{\text{sp}} \left(\frac{r_{\text{sp}}}{r} \right)^{\alpha}, \quad (5a)$$

$$\alpha = \frac{9 - 2\alpha_{\text{ini}}}{4 - \alpha_{\text{ini}}}, \quad (5b)$$

where ρ_{sp} is the normalization constant and r_{sp} is empirically defined by $r_{\text{sp}} \sim 0.2r_h$. The radius r_h is the distance of the gravitational influence of the central IMBH with the mass M_{BH} and is approximately obtained by $M(< r_h) = 4\pi \int_0^{r_h} \rho_{\text{DM}}(r) r^2 dr = 2M_{\text{BH}}$ [46]. The slope of the DM mini-spike takes the value $2.25 \leq \alpha \leq 2.5$ for $0 \leq \alpha_{\text{ini}} \leq 2$. In the case of an initially NFW profile, $\alpha_{\text{ini}} = 1$, this gives rise to $\alpha = 7/3$. If the initial profile of the mini-halo is a uniform distribution, then the final profile after the adiabatic growth of the IMBH would become a more gentle $\rho_{\text{spike}}(r) \propto (r/r_h)^{-3/2}$ [11, 33, 34].

It is important to note that the final profile of the DM mini-halo depends on the formation history of the central IMBH. If the IMBH has experienced disruptive processes such as mergers in the past, the mini-spike would be weakened or disappear. For this reason, we do not specify the value of the power-law index α of the DM mini-spike and treat it as a free parameter within the range $0 \leq \alpha \leq 3$. In the following, even if $\alpha < 2.25$, we will still call the DM distribution close to the central IMBH described by Eq. (5a) “a DM mini-spike” for the sake of simplicity. Indeed we will see that the “DM mini-spike” leaves its signature in the GW waveform when $\alpha \gtrsim 1.7$, but certainly does not when $\alpha = 0$. We will also assume different values of ρ_{sp} to study how the ambiguities in ρ_s and r_s mentioned above affect our results. Finally, we take r_{min} to be the innermost stable circular orbit of the central IMBH, $r_{\text{min}} = r_{\text{ISCO}} \equiv 6GM_{\text{BH}}/c^2$. It may be more precise to use $4GM_{\text{BH}}/c^2$ [35], but such a change of r_{min} does not alter at all the measurement accuracy of the DM parameters shown below. The parameters of the DM density profile are summarized in the table I below.

C. Candidate for a stellar mass object

Before moving onto the calculation of the GW waveform, we discuss what can be a candidate for “a stellar mass object”. Let us consider a stellar mass object with mass μ denoted by A , orbiting around an intermediate mass black hole B with mass M_{BH} . We consider the inspiral up to the the innermost stable circular orbit r_{ISCO}

$$r_{\text{ISCO}} = \frac{6GM_{\text{BH}}}{c^2} \simeq 9 \times 10^3 \text{km} \left(\frac{M_{\text{BH}}}{10^3 M_{\odot}} \right). \quad (6)$$

M_{DM}	M_{BH}	z_f	c_{halo}	r_{vir}
$10^6 M_{\odot}$	$10^3 M_{\odot}$	20	6.6	152.6pc
r_s	ρ_s	r_h	r_{sp}	ρ_{sp}
23.1pc	$3.8 \times 10^{-22} \text{g/cm}^3$	1.65pc	0.54pc	$226 M_{\odot}/\text{pc}^3$

TABLE I: Our reference model parameters of the IMBH, the DM mini-halo and the DM mini-spike. M_{DM} : The total mass of the mini-halo, M_{BH} : the mass of the central intermediate mass black hole, z_f : the formation redshift of the mini-halo, c_{halo} : the concentration of the mini-halo, r_{vir} : the virial radius of the mini-halo, r_s : the NFW r_s parameter of the mini-halo, ρ_s : the NFW ρ_s parameter of the mini-halo, r_h : the radius at which $M_{\text{DM}}(r_h) = 2M_{\text{BH}}$, r_{sp} : the radius where the spike forms (estimated by $r_{\text{sp}} = 0.2r_h$), and ρ_{sp} : the mini-halo mass density at r_{sp} .

Hence, the object A should have a radius smaller than at most 9×10^3 km. At the same time, the tidal radius of A orbiting B at the orbital radius of r_{ISCO} is

$$l_{A \text{ tidal}} \simeq r_{\text{ISCO}} \left(\frac{\mu}{M_{\text{BH}}} \right)^{1/3} \simeq 9 \times 10^2 \text{km} \left(\frac{\mu}{1M_{\odot}} \right)^{1/3} \left(\frac{M_{\text{BH}}}{10^3 M_{\odot}} \right)^{-1/3} \left(\frac{M_{\text{BH}}}{10^3 M_{\odot}} \right) \quad (7)$$

Hence, this object must be either a black hole or a neutron star. Alternatively, if we assume A to be a white dwarf of radius $l_A = 10000 \text{km}$ or a sun-like object of radius $l_A = 10^6 \text{km}$, the innermost orbital radius should be replaced by the radius below which the object A is tidally destroyed

$$r_{\text{tidal}} \simeq \left(\frac{M_{\text{BH}}}{\mu} \right)^{1/3} l_A \simeq 3 \times 10^{-7} \text{pc} \left(\frac{M_{\text{BH}}}{10^3 M_{\odot}} \right)^{1/3} \left(\frac{\mu}{1M_{\odot}} \right)^{-1/3} \left(\frac{l_A}{10^6 \text{km}} \right). \quad (8)$$

As will be stated, we will consider the orbital radius of order 10^{-8}pc or less, so we cannot assume our stellar mass object to be a normal star with radius $\sim 10^6 \text{km}$. A white dwarf may be an interesting candidate since an electromagnetic counterpart may be expected when it is tidally disrupted (e.g., [36–38]). Yet, here in this paper we assume a neutron star or a black hole when we refer to a stellar mass object.

III. GW WAVEFORM

A. Equation of motion for the stellar mass object

Let us consider a binary system which involves a small compact object with a mass of $\mu = 1M_{\odot}$ and an IMBH with a mass of $M_{\text{BH}} = 10^3 M_{\odot}$. The mass of the stellar mass object μ is much smaller than the mass of IMBH M_{BH} . So the reduced mass is approximately equal to μ and the barycenter position is approximately equal to the position of the IMBH. By adopting a reference frame attached to the barycenter, the equation of motion of the radial relative separation between the stellar mass object and the IMBH describes the motion of the former and is given by

$$\frac{d^2 r}{dt^2} = -\frac{GM_{\text{eff}}}{r^2} - \frac{F}{r^{\alpha-1}} + \frac{h^2}{r^3}, \quad (9)$$

where h is the angular momentum of the stellar mass object per its mass, and M_{eff} and F are defined by

$$M_{\text{eff}} = \begin{cases} M_{\text{BH}} - M_{\text{DM}}(< r_{\text{min}}) & (r_{\text{min}} \leq r \leq r_{\text{sp}}), \\ M_{\text{BH}} & (r < r_{\text{min}}), \end{cases} \quad (10a)$$

$$F = \begin{cases} r_{\text{min}}^{\alpha-3} M_{\text{DM}}(< r_{\text{min}}) & (r_{\text{min}} \leq r \leq r_{\text{sp}}), \\ 0 & (r < r_{\text{min}}). \end{cases} \quad (10b)$$

The mass $M_{\text{DM}}(< r_{\text{min}})$ denotes the DM mass contained within the ISCO and is defined as $M_{\text{DM}}(< r_{\text{min}}) \equiv 4\pi r_{\text{sp}}^{\alpha} \rho_{\text{sp}} r_{\text{min}}^{3-\alpha} / (3-\alpha)$. The first term on the right-hand side of Eq. (9) describes the gravitational potential of the effective mass of the central IMBH which is modified by the DM due to the absence of the DM within the ISCO, the second term accounts for the DM effect, and the third term represents a centrifugal force. Here the dynamical friction force and the GW back reaction force are neglected because these effects are much smaller than the gravitational potential of the IMBH. We will introduce these effects to include an adiabatic evolution of the orbital radius in the next subsection.

We assume that the stellar mass object orbits in a circular manner for simplicity. The orbital radius R is obtained by solving $d^2 r / dt^2 = 0$ in Eq. (9). The orbital frequency ω_s is related to the angular momentum h by $R\omega_s$, so we get

$$\omega_s = \left[\frac{GM_{\text{eff}}}{R^3} + \frac{F}{R^{\alpha}} \right]^{1/2}. \quad (11)$$

When a DM mini-spike is not present around the IMBH, $F \rightarrow 0$ and $M_{\text{eff}} \rightarrow M_{\text{BH}}$, so Eq. (11) leads to the Kepler's law $\omega_s^2 = GM_{\text{BH}}/R^3$.

B. Energy balance equation

In this subsection, we introduce the GW back-reaction and the dynamical friction into the stellar mass object's orbit by taking the energy balance equation into account. When the stellar mass object orbits around the IMBH, a part of its energy E_{orbit} is converted into GW emission loss E_{GW} and dynamical friction loss E_{DF} . Thus the following energy balance equation is satisfied:

$$-\frac{dE_{\text{orbit}}}{dt} = \frac{dE_{\text{GW}}}{dt} + \frac{dE_{\text{DF}}}{dt}. \quad (12)$$

As we will see in this subsection, this energy balance equation gives the time evolution of the orbital radius. The resulting orbit can be regarded as a quasi-circular orbit because of the smallness of these dissipative effects.

The orbital energy E_{orbit} is the sum of the kinetic energy and the gravitational potential of the stellar mass object, so we can calculate E_{orbit} using Eq. (11),

$$\begin{aligned} E_{\text{orbit}} &= \frac{1}{2}\mu v^2 + \frac{h^2}{2R^2} - \frac{G\mu M_{\text{eff}}}{R} \\ &= -\frac{G\mu M_{\text{eff}}}{2R} + \frac{4-\alpha}{2(2-\alpha)} \frac{\mu F}{R^{\alpha-2}}, \end{aligned} \quad (13)$$

where v is the orbital velocity. When we consider the evolution of the radius R , dR/dt does not vanish. So the time derivative of Eq. (13) gives the following equation,

$$\frac{dE_{\text{orbit}}}{dt} = \left(\frac{GM_{\text{eff}}}{2R^2} + \frac{4-\alpha}{2} \frac{F}{R^{\alpha-1}} \right) \mu \frac{dR}{dt}. \quad (14)$$

To the lowest order in the Post Newtonian expansion, the gravitational radiation energy is given by the quadrupole formula. We apply the formula to the circular Newtonian binary and obtain

$$\frac{dE_{\text{GW}}}{dt} = \frac{32}{5} \frac{G\mu^2}{c^5} R^4 \omega_s^6. \quad (15)$$

When the stellar mass object moves through the cloud of DM, it gravitationally interacts with DM particles. This effect is called dynamical friction, sometimes referred to as gravitational drag which was first discussed by Chandrasekar [39]. Because of dynamical friction, the stellar mass object running through the DM halo is decelerated in the direction of its motion and loses its kinetic energy as well as its angular momentum. The dynamical friction force is given by $f_{\text{DF}} = 4\pi G^2 \mu^2 \rho_{\text{DM}}(r) \ln \Lambda / v^2$ where v is the velocity of the stellar mass object [40]. The Coulomb logarithm Λ is defined by $\lambda \cong b_{\text{max}} v_{\text{typ}}^2 / (G\mu)$ where b_{max} is the maximum impact parameter and v_{typ} is the typical velocity of the stellar mass object. We take $\ln \Lambda \cong 3$. From the expression of the dynamical friction force, we obtain the friction loss,

$$\frac{dE_{\text{DF}}}{dt} = v f_{\text{DF}} = 4\pi G^2 \frac{\mu^2 \rho_{\text{DM}}(r)}{v} \ln \Lambda. \quad (16)$$

To find the numerical solution of the energy balance equation (12) easily, we introduce a dimensionless radius parameter x defined by

$$x \equiv \varepsilon^{1/(3-\alpha)} R, \quad (17)$$

with

$$\varepsilon \equiv \frac{F}{GM_{\text{eff}}}. \quad (18)$$

Using the above definition of x , the energy balance equation (12) can be rewritten in the form of the differential equation of x with respect to time t as

$$\frac{dx}{dt} = -c_{\text{GW}} \frac{(1+x^{3-\alpha})^3}{4x^3 [1+(4-\alpha)x^{3-\alpha}]} - c_{\text{DF}} \frac{1}{(1+x^{3-\alpha})^{1/2} [1+(4-\alpha)x^{3-\alpha}] x^{-5/2+\alpha}}, \quad (19)$$

where the coefficients are defined by

$$c_{\text{GW}} \equiv \frac{256}{5} \left(\frac{G\mu}{c^3} \right) \left(\frac{GM_{\text{eff}}}{c} \right)^2 \varepsilon^{4/(3-\alpha)}, \quad (20a)$$

$$c_{\text{DF}} \equiv (8\pi G^2 \mu \rho_{\text{sp}} r_{\text{sp}}^\alpha \ln \Lambda) (GM_{\text{eff}})^{-3/2} \varepsilon^{(2\alpha-3)/[2(3-\alpha)]}. \quad (20b)$$

The coefficient c_{GW} is related to the gravitational radiation energy and the coefficient c_{DF} is related to the dynamical friction. In the case of the initially NFW profile, $\alpha = 7/3$, the coefficients c_{GW} and c_{DF} are $c_{\text{GW}} = 2.0 \times 10^{-33}$ [1/year], $c_{\text{DF}} = 2.1 \times 10^{-8}$ [1/year]. Note that the dynamical friction coefficient c_{DF} is much larger than the gravitational radiation coefficient c_{GW} .

C. GW waveform

The GW waveform from the binary composed of two compact objects with masses μ and M_{BH} is given by

$$h_+(t) = \frac{1}{D} \frac{4G\mu\omega_s^2 R^2}{c^4} \frac{1 + \cos^2 \iota}{2} \cos(\omega_{\text{GW}} t), \quad (21a)$$

$$h_\times(t) = \frac{1}{D} \frac{4G\mu\omega_s^2 R^2}{c^4} \cos \iota \sin(\omega_{\text{GW}} t), \quad (21b)$$

where D is the distance to the source (luminosity distance for a cosmological source), R is the orbital radius, ι is the inclination angle, which is the angle between the line-of-sight and the rotational axis of the orbits, and ω_{GW} is the GW frequency which is given by $\omega_{\text{GW}} \equiv 2\omega_s$ [41].

The waveforms Eqs. (21a) and (21b) are derived on the assumption that the motion of the source is described by a circular Newtonian orbit. But in fact, the radius R and the frequency ω_s are not constant because the orbital energy E_{orbit} decreases gradually due to both dynamical friction and the GW back-reaction. Including these effects, the orbit shrinks adiabatically and becomes a quasi-circular orbit. So the radius R and the frequency ω_s should be replaced by $R \rightarrow R(t)$, $\omega_s \rightarrow \omega_s(t)$ and the phase $\omega_{\text{GW}} t$ should also be replaced by $\omega_{\text{GW}} t \rightarrow \Phi(t)$ as defined by Eq. (22c) below. Thus, the GW waveform is expressed by

$$h_+(t) = \frac{1}{D} \frac{4G\mu\omega_s(t)^2 R(t)^2}{c^4} \frac{1 + \cos^2 \iota}{2} \cos[\Phi(t)], \quad (22a)$$

$$h_\times(t) = \frac{1}{D} \frac{4G\mu\omega_s(t)^2 R(t)^2}{c^4} \cos \iota \sin[\Phi(t)], \quad (22b)$$

$$\Phi(t) \equiv \int^t \omega_{\text{GW}}(t') dt'. \quad (22c)$$

In order to discuss detectability and parameter accuracy in GW observations, it is convenient to work in the frequency domain. The Fourier transformation of the GW waveform is given by

$$\tilde{h}_{+, \times}(f) = \int_{-\infty}^{\infty} h_{+, \times}(t) e^{2\pi i f t} dt, \quad (23)$$

where f is the GW frequency. For simplicity, we consider a GW coming in the detector from the optimal direction for $+$ mode. In such a situation, detector pattern function are $F_+ = 1$ and $F_\times = 0$. So the response of the detector to the GW is $h(t) = h_+(t)$. Using Eq. (22a), we rewrite the GW waveform as

$$h(t) = A(t_{\text{ret}}) \cos \Phi(t_{\text{ret}}), \quad (24a)$$

$$A(t) \equiv \frac{1}{D} \frac{4G\mu\omega_s^2(t) R^2(t)}{c^4} \frac{1 + \cos^2 \iota}{2}, \quad (24b)$$

where $A(t)$ is the time-dependent amplitude and $\Phi(t)$ is the time-dependent GW phase. In the above equations, we have introduced the retarded time $t_{\text{ret}} \equiv t - D/c$. In the range of frequency we are concerned with, the time-dependent amplitude $A(t)$ varies slowly, while the time-dependent phase $\Phi(t)$ varies rapidly. So, the Fourier transformation of the GW waveform can be calculated approximately using the stationary phase method. In this method, the rapidly oscillating term is neglected and only the slowly oscillating term survives. Then the GW waveform in the Fourier domain becomes

$$\tilde{h}(f) = \frac{1}{2} e^{i\Psi(t)} A(t) \left[\frac{2\pi}{\ddot{\Phi}(t)} \right]^{1/2}, \quad (25a)$$

$$\Psi(t) = 2\pi f \frac{D}{c} + \tilde{\Phi}(t) - \frac{\pi}{4}, \quad (25b)$$

$$\tilde{\Phi}(t) \equiv 2\pi f t - \Phi(t), \quad (25c)$$

where the time t is related to frequency by $2\pi f = \omega_{\text{gw}}(t)$.

As we will discuss in Appendix A, the GW waveform Eqs. (25a), (25b) and (25c) can be rewritten explicitly in the frequency domain as follows:

$$\tilde{h}(f) = \mathcal{A} f^{-7/6} e^{i\Psi(f)} \chi^{19/4} [K(x)(1 + \tilde{c}J(x))]^{-1/2}, \quad (26a)$$

$$\mathcal{A} = \left(\frac{5}{24}\right)^{1/2} \frac{1}{\pi^{2/3}} \frac{c}{D} \left(\frac{GM_c}{c^3}\right)^{5/6} \frac{1 + \cos^2 \iota}{2}, \quad (26b)$$

$$\Psi(f) = 2\pi f \tilde{t}_c - \Phi_c - \frac{\pi}{4} - \tilde{\Phi}(f), \quad (26c)$$

$$\tilde{\Phi}(f) = \frac{10}{3} \left(\frac{8\pi GM_c}{c^3}\right)^{-5/3} \left[-f \int_{\infty}^f df' \frac{\chi^{11/2}}{f'^{11/3} K(1 + \tilde{c}J)} + \int_{\infty}^f df' \frac{\chi^{11/2}}{f'^{8/3} K(1 + \tilde{c}J)} \right], \quad (26d)$$

$$J(x) = \frac{4x^{11/2-\alpha}}{(1+x^{3-\alpha})^{7/2}}, \quad (26e)$$

$$K(x) = \frac{(1+x^{3-\alpha})^{5/2} (1 + \alpha x^{3-\alpha}/3)}{1 + (4-\alpha)x^{3-\alpha}}, \quad (26f)$$

$$\chi = (\delta\varepsilon)^{1/(\alpha-3)} x, \quad (26g)$$

$$\delta = \left(\frac{GM_{\text{eff}}}{\pi^2 f^2}\right)^{(3-\alpha)/3}, \quad (26h)$$

where \mathcal{A} is the overall amplitude, M_c is the chirp mass defined by $M_c \equiv \mu^{3/5} M_{\text{eff}}^{5/2}$, \tilde{t}_c is the sum of the binary coalescence time t_c and D/c , Φ_c is the phase at coalescence, α is the power-law index of the DM mini-spike, \tilde{c} is defined by $\tilde{c} \equiv c_{\text{DF}}/c_{\text{GW}}$, δ is a new frequency variable, x is defined in Eq. (17), and ε is defined by Eq. (18). The DM information is encoded in the waveform Eq. (28a) through $K(x)$, $J(x)$, χ , \tilde{c} and M_{eff} . So if we take $K(x) \rightarrow 1$, $\chi \rightarrow 1$, $\tilde{c} \rightarrow 0$, $M_{\text{eff}} \rightarrow M_{\text{BH}}$, then Eq. (28a) becomes the waveform without the DM shown in Eqs. (A15a)-(A15d).

D. $\delta\varepsilon$ expansion

As we will discuss in the next section, we consider a five-year observation by eLISA which corresponds to $f \gtrsim 10^{-3}\text{Hz}$. In this setup, $\delta\varepsilon \ll 1$ is satisfied. For example, we get $\delta\varepsilon = 3.5 \times 10^{-6}$ for $\alpha = 7/3$, $f = 0.01\text{Hz}$, $\mu = 1M_{\odot}$ and the parameters ρ_{sp} , r_{sp} , and M_{BH} listed in the table I. So $\delta\varepsilon$ can be treated as a small expansion parameter. Since the measurement errors of the physical parameters contained in GW are much more sensitive to the GW phase rather than its amplitude, we expand the GW waveform $\tilde{h}(f)$ up to the first order in $\delta\varepsilon$ in the phase and up to the zero-th order in the amplitude. Using an expansion of χ in $\delta\varepsilon$,

$$\chi = 1 + \frac{1}{3}\delta\varepsilon + \frac{2-\alpha}{9}\delta^2\varepsilon^2 + \dots, \quad (27)$$

the GW waveform given by Eqs. (26a)-(26h) becomes

$$\tilde{h}(f) = \mathcal{A} f^{-7/6} e^{i\Psi(f)} L(f)^{-1/2}, \quad (28a)$$

$$\mathcal{A} = \left(\frac{5}{24}\right)^{1/2} \frac{1}{\pi^{2/3}} \frac{c}{D} \left(\frac{GM_c}{c^3}\right)^{5/6} \frac{1 + \cos^2 \iota}{2}, \quad (28b)$$

$$\tilde{\Phi}(f) = \frac{10}{3} \left(\frac{8\pi GM_c}{c^3}\right)^{-5/3} \left[-f \int_{f_{\text{ISCO}}}^f df' f'^{-11/3} L^{-1}(f') + \int_{f_{\text{ISCO}}}^f df' f'^{-8/3} L^{-1}(f') \right], \quad (28c)$$

$$L(f) = 1 + 4c_{\varepsilon} \tilde{\delta}^{(11-2\alpha)/[2(3-\alpha)]}, \quad (28d)$$

$$\tilde{\delta} = \left(\frac{G}{\pi^2 f^2}\right)^{(3-\alpha)/3}, \quad (28e)$$

$$c_{\varepsilon} = M_{\text{eff}}^{(11-2\alpha)/6} \tilde{c}_{\varepsilon}^{(11-2\alpha)/[2(3-\alpha)]}, \quad (28f)$$

where the overall amplitude \mathcal{A} is defined by Eq. (26b) and $\Psi(f)$ is defined by Eq. (26c). The upper bound of the integration in Eq. (28c), $f_{\text{ISCO}} > f$ in the eLISA frequency band, is the GW frequency when the stellar mass object enters the innermost stable circular orbit. Hence, $\tilde{\Phi}(f)/(2\pi)$ is in essence the GW cycles from the frequency f to the coalescence. The post-Newtonian (PN) effects which are neglected in the above equations must be taken into account in real data analysis. However, the frequency-dependence of the PN effect in the GW phase $\tilde{\Phi}(f)$ differs from that of the DM effect which depends on the power-law index α . So, the measurement

accuracies of the DM parameters as we will discuss later would not be affected seriously by higher order terms in the PN expansion.

Until the previous sections, we have included both the dynamical friction and the gravitational pull of the DM mini-spike. It is easily shown that the dynamical effect has much more impact on the measurement accuracy of the DM parameters than the DM mini-spike does [25], and the above expression indeed includes the dynamical friction but not the gravitational pull of the DM mini-spike. In fact, within the approximation in this subsection and the following, the gravitational potential of the DM mini-spike shows its signature only in the IMBH mass redefinition ($M_{\text{BH}} \rightarrow M_{\text{eff}}$ in M_c in the above equations). We however note that even such a tiny effect as the gravitational pull of the DM mini-spike do affect the detectability of GW thanks to the large number of the GW cycles in the eLISA detection band [23].

It is important to note that the DM parameters appear only in α and c_ϵ and that they are contained in the GW phase $\tilde{\Phi}(f)$. We make use of the above equations to calculate measurement errors of the waveform parameters in the next section. We also define the phase difference $\Delta\tilde{\Phi}(f)$ by

$$\Delta\tilde{\Phi}(f) \equiv \tilde{\Phi}(f) - \tilde{\Phi}_0(f), \quad (29)$$

where $\tilde{\Phi}(f)$ defined by Eq. (28c) is the phase including the DM effect and $\tilde{\Phi}_0(f)$ defined by Eq. (A15d) is the phase without the DM effect. $\Delta\tilde{\Phi}(f)$ is shown in Fig. 1 which indicates that the phase difference becomes significant for large α and for the large GW frequency f . This is because in this case, the DM density near the central BH increases and the effect of the DM on the motion of the stellar mass object is significant. As we discussed in our previous paper [23], the phase difference causes the mismatch between the waveform including the DM effect and the waveform without the DM effect. The phase difference $\Delta\tilde{\Phi}(f)$ typically above 1 indicates the necessity to use the waveform including the DM effect as a template. As can be seen in Fig. 1, if the template without the DM effect is applied to the GW signal including the effect induced by the DM with $\alpha > 1.5$, the resulting S/N would degrade significantly.

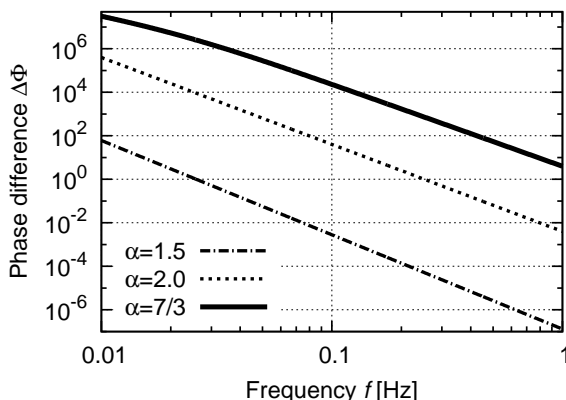


FIG. 1: The accumulated phase difference $\Delta\tilde{\Phi}$ against the power-law index α , defined by Eq. (29). In essence, this is the difference between the accumulated phase from GW frequency f and the binary coalescence with and without the DM mini-spike. Three different curves show $\Delta\tilde{\Phi}$ for three different values of α . For instance, if detecting a binary GW from $f = 0.01\text{Hz}$ to its coalescence, we would observe by a factor of 10^7 more GW cycles in the case with a $\alpha = 7/3$ DM mini-spike than without any. For this plot, we take $\mu = 1M_\odot$ and $\rho_{\text{sp}}, r_{\text{sp}},$ and M_{BH} are as listed in the table I.

IV. PARAMETER RESOLUTION FOR ELISA

A. Brief review of the Fisher analysis

In this subsection, we give a brief review of parameter estimation (see [42, 43] for more details). Let us consider detecting GWs with a single detector. The detector output $s(t)$ can be written by the sum of the GW signal $h(t)$ and detector noise $n(t)$:

$$s(t) = h(t) + n(t). \quad (30)$$

Assuming that the detector noise is stationary, the correlation between different Fourier components of the noise is expressed as

$$\langle \tilde{n}(f) \tilde{n}^*(f') \rangle = \frac{1}{2} \delta(f - f') S_n(f), \quad (31)$$

where the angled brackets $\langle \rangle$ denote an ensemble average, the asterisk is complex conjugation and $S_n(f)$ is a one-sided power spectral density of the detector noise. In this paper, we consider the GW observation using eLISA which has the best sensitivity at around $f = 0.01$ [Hz]. The noise spectral density of eLISA is given by

$$S_n(f) = \frac{20}{3} \frac{4S_{\text{acc}}(f)/(2\pi f)^4 + S_{\text{sn}}(f) + S_{\text{omn}}(f)}{\ell^2} \left[1 + \left(\frac{f}{0.41c/2\ell} \right) \right]^2, \quad (32a)$$

where $S_{\text{acc}}(f) = 2.13 \times 10^{-29} (1 + 10^{-4}/f)$ [$\text{m}^2/\text{s}^4\text{Hz}$] is the acceleration noise spectral density, $S_{\text{sn}}(f) = 6.28 \times 10^{-23}$ [m^2/Hz] is the shot noise spectral density, $S_{\text{omn}}(f) = 5.25 \times 10^{-23}$ [m^2/Hz] is the other measurement noise spectral density and $\ell = 10^9$ [m] is the separation between the spacecraft which is the length of its arms of the laser interferometer (see [21, 44] for details).

It is convenient to introduce a noise-weighted inner product between two signals $h_1(t)$ and $h_2(t)$ by

$$(h_1|h_2) \equiv 4\text{Re} \int_{f_{\text{ini}}}^{f_{\text{ISCO}}} \frac{\tilde{h}_1(f) \tilde{h}_2^*(f)}{S_n(f)} df, \quad (33)$$

where Re denotes the real part and f_{ini} is the initial frequency. Assuming that the detector noise is Gaussian and stationary, the probability density of the detector noise is described by $p(n) \propto e^{-(n|n)/2}$. We can rewrite this expression in the form of detector signal $s(t)$ and GWs signal $h(t)$ using Eq. (30) as $p(n) \propto e^{-(s-h|s-h)/2}$.

In the above case, $h(t)$ is known, while in actual GW experiments, $h(t)$ should be replaced with a template $h(t; \theta)$, where $\theta = \{\theta_1, \dots, \theta_N\}$ is a collection of unknown parameters. To determine the waveform parameters θ , it is necessary to search for the parameters which minimize the logarithm of the maximum likelihood ratio, $(s-h|s-h) - (s|s)$. As a result of this process, we can infer the values of θ . However, the expected values have statistical errors because the detector noise is a random process. These measurement errors $\Delta\theta^i$ of the waveform parameters are approximately described by the Gaussian probability distribution for large S/N ,

$$p(\Delta\theta^i) = \mathcal{N} \exp\left(-\frac{1}{2} \Gamma_{ij} \Delta\theta^i \Delta\theta^j\right), \quad (34)$$

where \mathcal{N} is the normalization factor and Γ_{ij} is called the Fisher information matrix defined by

$$\Gamma_{ij} \equiv \left\langle \frac{\partial h}{\partial \theta^i} \middle| \frac{\partial h}{\partial \theta^j} \right\rangle. \quad (35)$$

The inverse of the Fisher matrix gives the root-mean-square (rms) errors of the waveform parameters θ^i :

$$\Delta\theta^i \equiv \sqrt{\langle (\Delta\theta^i)^2 \rangle} = \sqrt{(\Gamma^{-1})_{ii}}, \quad (36)$$

where $(\Gamma^{-1})_{ii}$ denotes the diagonal elements of the inverse Fisher matrix.

B. Preparation for parameter estimation

The inspiral GW waveform from the IMBH surrounded by the DM mini-spike is described by six parameters which appear in Eqs. (28a) - (28f): the overall amplitude, \mathcal{A} ; the time constant, $\tilde{t}_c \equiv t_c + D/c$, which is the sum of the traveling time D/c and the coalescence time t_c ; the coalescence phase, Φ_c ; the chirp mass, M_c ; the two DM parameters, α and c_ε . Note that the beam pattern function of eLISA is neglected here because we are concerned with how the DM parameters are determined by GW observations but not with the angular resolution of eLISA (see [45] for discussion of angular resolution).

The inner product between the derivatives of the waveform with respect to the parameters θ yields the values of the Fisher matrix elements. The derivatives with respect to \mathcal{A} , \tilde{t}_c , Φ_c and $\ln M_c$ are calculated straightforwardly as follows:

$$\frac{\partial \tilde{h}}{\partial \ln \mathcal{A}} = \tilde{h}, \quad (37a)$$

$$\frac{\partial \tilde{h}}{\partial \tilde{t}_c} = 2\pi i f \tilde{h}, \quad (37b)$$

$$\frac{\partial \tilde{h}}{\partial \Phi_c} = -i \tilde{h}, \quad (37c)$$

$$\frac{\partial \tilde{h}}{\partial \ln M_c} = \frac{5}{3} i \tilde{h} \tilde{\Phi}. \quad (37d)$$

The derivatives with respect to the DM parameters α, c_ε are obtained by applying the chain rule to the following equations:

$$\frac{\partial \tilde{h}}{\partial \ln \alpha} = \alpha \tilde{h} \left(i \frac{\partial \Psi}{\partial \alpha} - \frac{1}{2} \frac{1}{L} \frac{\partial L}{\partial \alpha} \right), \quad (38a)$$

$$\frac{\partial \tilde{h}}{\partial \ln c_\varepsilon} = c_\varepsilon \tilde{h} \left(i \frac{\partial \Psi}{\partial c_\varepsilon} - \frac{1}{2} \frac{1}{L} \frac{\partial L}{\partial c_\varepsilon} \right), \quad (38b)$$

where L is defined in Eq. (28d). However, since the explicit expressions are complicated, we take the derivatives numerically.

Next, we derive the initial frequency at which the GW observation starts. In the presence of the DM mini-spike, the stellar mass object orbiting the central IMBH loses its angular momentum gradually due both to the dynamical friction and GW radiation reaction. So the coalescence arises earlier than the case without the DM. Time evolution of the frequency is described by Eq. (A12),

$$\frac{df}{d\tau} = -\frac{3}{5}\pi \left(\frac{f}{f_0} \right)^{5/3} f^2 \chi^{-11/2} [K(1 + \tilde{c}J)], \quad (39)$$

where $f_0 \equiv c^3/8\pi GM_c$ and τ is the time to the coalescence. (Note that $d\tau = -dt$.) The lower bound $f_{\text{ini}}(\alpha)$ of the integral in Eq. (33) is required for calculating the inner product in the Fisher matrix. Given that the GW is observed by eLISA for 5 years prior to the coalescence, this bound is obtained by

$$f_{\text{ini}}(\alpha) \equiv f(\alpha, \tau = 5 \text{ [yr]}). \quad (40)$$

By numerically solving Eq. (39), we show the dependence of α on f_{ini} in Fig. 2. This figure indicates that the DM mini-spike affects more strongly the motion of the stellar mass object for larger α . The initial frequency for a 5 year observation is almost constant for small α due to the smallness of the effect of the DM. Conversely, the initial frequency drops sharply for large α due to the dynamical friction from the DM.

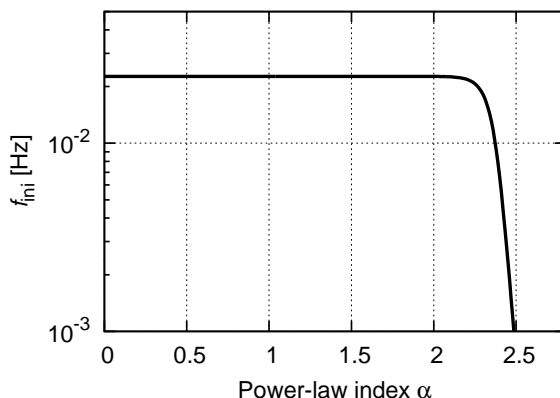


FIG. 2: Initial frequency against the power-law index α . We assume that the GW is detected by an eLISA 5 year observation. For small α , f_{ini} is almost constant. On the other hand, for large α , f_{ini} drops sharply due mainly to the dynamical friction. For this plot, we take $\mu = 1M_\odot$ and $\rho_{\text{sp}}, r_{\text{sp}}$, and M_{BH} are as listed in the table I.

C. Measurement accuracy: The case for initially NFW profile

In this section, we consider the most likely case that the DM mini-spike has an initially NFW profile, $\alpha = 7/3$. Derivatives of the waveform with respect to the parameters given by Eqs. (37a)-(38b) are calculated numerically. Substitution of these results into Eqs. (35) and (36) gives rise to the rms errors $\Delta \ln \mathcal{A}$, $\Delta \tilde{t}_c$, $\Delta \Phi_c$, $\Delta \ln M_c$, $\Delta \ln \alpha$ and $\Delta \ln c_\varepsilon$ as follows.

$$\frac{\Delta \mathcal{A}}{\mathcal{A}} = 0.1 \left(\frac{10}{S/N} \right), \quad (41a)$$

$$\Delta \tilde{t}_c = 1.0 \text{ [s]} \left(\frac{10}{S/N} \right), \quad (41b)$$

$$\Delta \Phi_c = 1.3 \text{ [rad]} \left(\frac{10}{S/N} \right), \quad (41c)$$

$$\frac{\Delta M_c}{M_c} = 3.1 \times 10^{-7} \left(\frac{10}{S/N} \right), \quad (41d)$$

$$\frac{\Delta \alpha}{\alpha} = 1.2 \times 10^{-6} \left(\frac{10}{S/N} \right), \quad (41e)$$

$$\frac{\Delta c_\varepsilon}{c_\varepsilon} = 5.9 \times 10^{-5} \left(\frac{10}{S/N} \right). \quad (41f)$$

Here we take ρ_{sp} , r_{sp} , and M_{BH} from table I and $\mu = 1M_\odot$. These measurement errors are inversely proportional to S/N . So the waveform parameters are measurable with better accuracy for larger GW signals. A notable feature of the above results is that the chirp mass M_c and the two DM parameters α and c_ε are determined much more accurately than the overall amplitude \mathcal{A} , the coalescence time t_c and the coalescence phase Φ_c . This fact reflects that M_c , α and c_ε appear in the phase of the waveform $\tilde{\Phi}(f)$. From Eqs. (B1), (22c) and (25c), the GW phase is proportional to the number of GW cycles which amplify the sensitivity to the parameters which appear in the phase $\tilde{\Phi}(f)$ by a factor N_{cycles} . Thus, the fractional error of the chirp mass which is proportional to the phase is order of $1/N_{\text{cycle}}$ and the two DM parameters are also determined very accurately. In fact, Fig. 8 indicates the value of $1/N_{\text{cycle}}$ is about 10^{-7} , which is consistent with the value of $\Delta M_c/M_c$ in Eq. (41d).

We also investigate the correlation between the parameters which appear in the phase, M_c , α and c_ε . Figure. 3 illustrates the Fisher ellipses for M_c , α and c_ε in $S/N = 10$. From the figures, we observe that M_c , α and c_ε are strongly correlated with each other because all of them are contained in the phase. However, they are not completely degenerate and are determined independently. This fact can be traced to the difference of the frequency-dependence between M_c , α and c_ε .

In the above discussion, the mass of the central IMBH M_{BH} and that of the stellar mass object μ are fixed. Next we analyze the measurement errors for various values of μ and M_{BH} . The results are shown in Fig. 4. The figure indicates the errors of the parameters in the phase $\tilde{\Phi}(f)$ increase linearly with the stellar mass object mass μ . This behavior comes from the fact that the number of cycles N_{cycle} decreases in proportion to the stellar mass object mass μ . Similarly, the larger is the mass of the IMBH, the smaller the number of the orbital cycles the stellar mass object experienced in the five years prior to the coalescence within the eLISA band. For this reason, the measurement errors in M_c , α , and c_ε increase for a larger IMBH mass as can be seen in Fig. 4.

D. Measurement accuracy: General case for initial DM profile

We now extend the analysis in the previous section where we considered the case of the initially NFW profile. We next consider the general case without specifying the value of α with M_{BH} , ρ_{sp} , and r_{sp} fixed to the values quoted in the table I. The rms errors depend on the DM power-law index α . We show $\Delta \ln M_c$, $\Delta \ln \alpha$ and $\ln \Delta c_\varepsilon$ in Fig. 5.

As shown in Fig. 5, the accuracy of the DM parameters $\Delta \ln \alpha$ and $\Delta \ln c_\varepsilon$ are better for the larger α . This is because steeper density distributions contain more DM mass within the orbital radius (see Fig. 2 in [23]). In other words, the steeper density distribution has more impact on the motion of the stellar mass object and the GW waveform is modified more strongly by the DM mini-spike. So the DM information can be extracted from the GW waveform if the DM mini-halo near the BH has a steep profile.

On the other hand, the measurement accuracy of the parameters which appear in the phase $\tilde{\Phi}(f)$ become worse in $\alpha > 2.5$. This feature can be explained by the number of GW cycles N_{cycle} which will be discussed in the Appendix B. There we show that N_{cycle} falls sharply at $\alpha \sim 2.5$ (See Fig. 8). The sensitivity to the parameters which appear in the phase $\tilde{\Phi}(f)$ is amplified by the number of cycles N_{cycle} in the frequency bandwidth of eLISA. For this reason, the measurement errors of M_c , α and c_ε increase suddenly at $\alpha \sim 2.5$, as is shown in Fig. 5. We also note that this figure shows that we can measure the power-law index α at 10 % level even for a moderately flat radial distribution with $\alpha \sim 1.7$. In fact, when considering the gravitational pull due to the DM potential only, it affects detectability of GW signals only for $\alpha \gtrsim 2$. It is the dynamical friction that enables us to explore a flatter DM distribution than “a DM mini-spike” referred in the literature that has $\alpha \geq 2.25$.

Figure 6 shows the relative errors of the DM parameters, α and c_ε for various values of ρ_{sp} as a function of α . As can be seen in Fig. 6, the relative errors for the fixed α become smaller approximately linearly as the DM density increases. This behaviour can be traced to the amount of the DM within the orbital radius of the stellar mass object. It should be noted that the value of ρ_{sp} we adopt in this paper is derived under the assumption that the initial DM mini-halo profile is the NFW profile as discussed in the section II. Even if the DM density is an order of magnitude more sparse than that indicated by the NFW profile, the power-law index α is measurable with an accuracy of $\Delta\alpha/\alpha < 10\%$ for $\alpha > 1.9$.

V. CONCLUSION

In this paper, we have investigated the measurement accuracy of dark matter (DM) parameters by gravitational (GW) observations. We consider a binary system composed of an intermediate mass black hole (IMBH)

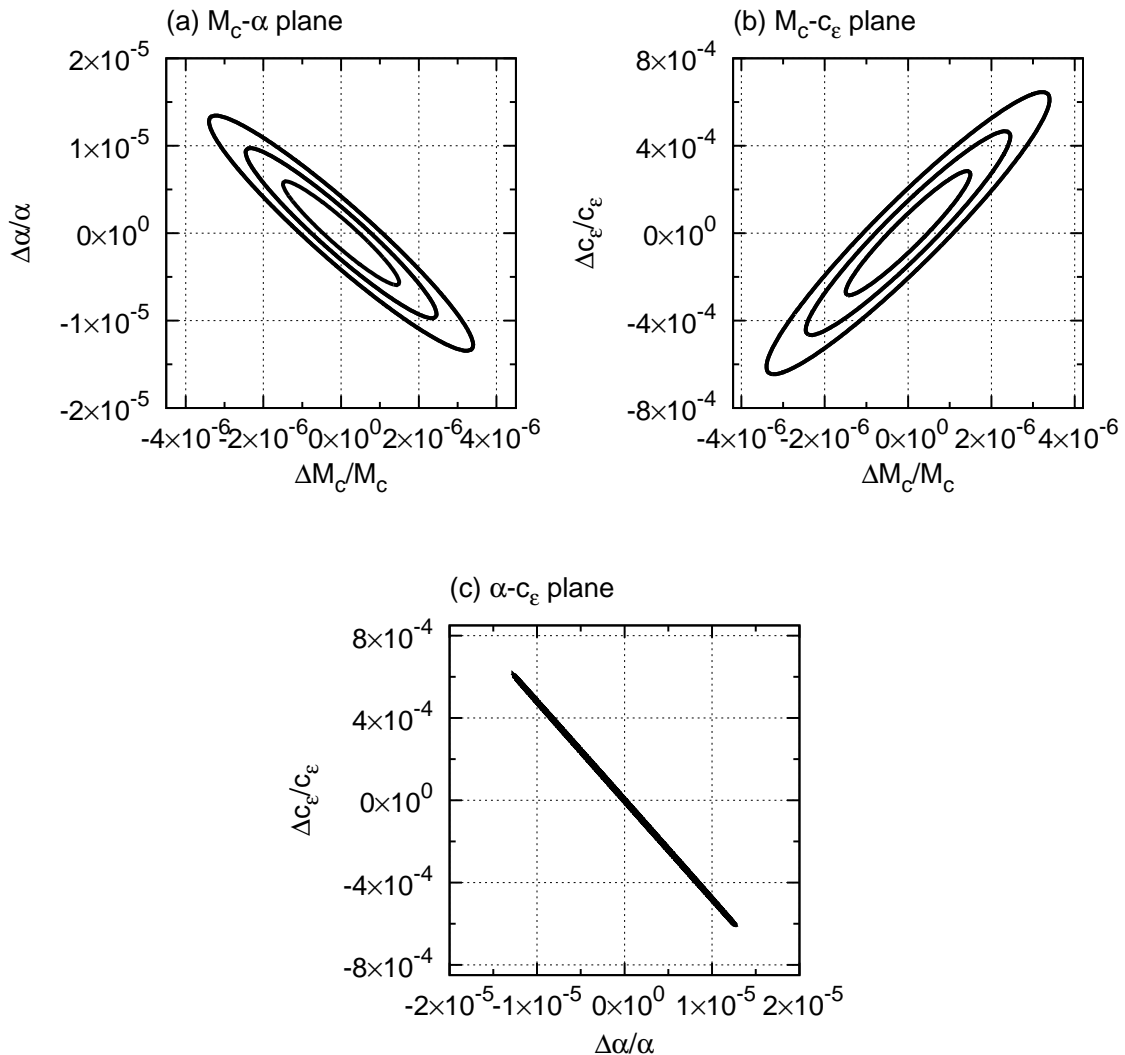


FIG. 3: Confidence level contours of 68.3%, 95.4% and 99.7% for $S/N = 10$ in the case where the initial DM halo has an NFW profile and the final profile has the radial power-law index of $\alpha = 7/3$ through an adiabatic growth. We assume ρ_{sp} , r_{sp} , and M_{BH} from the table I and $\mu = 1M_\odot$.

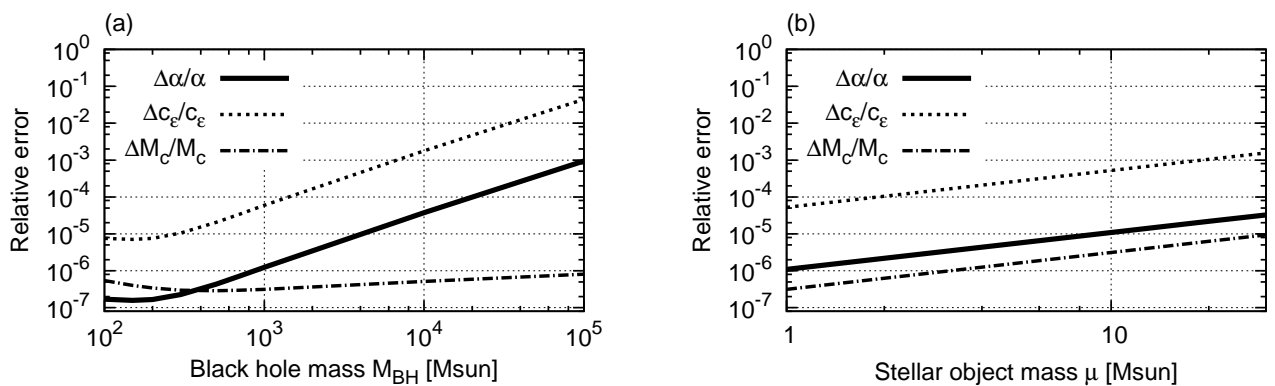


FIG. 4: The relative errors of the parameters in the phase $\tilde{\Phi}(f)$ versus (a) the central BH mass M_{BH} and (b) the stellar mass object mass μ for $S/N = 10$ and $\alpha = 7/3$. For this plot, ρ_{sp} and r_{sp} are taken from the table I. The other parameter is fixed to be $\mu = 1M_\odot$ in the left and $M_{\text{BH}} = 10^3 M_\odot$ in the right, respectively. Note that the both axes are in the logarithmic scales. The solid line, the dashed line, the dashed-dotted line correspond to $\Delta\alpha/\alpha$, $\Delta c_\epsilon/c_\epsilon$, $\Delta M_c/M_c$ respectively.

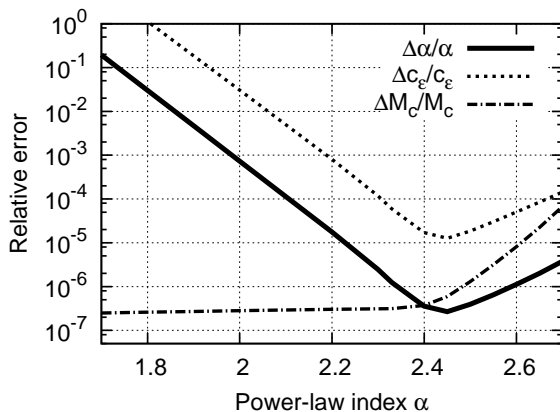


FIG. 5: The relative errors of the parameters in the phase $\tilde{\Phi}(f)$ versus the power-law index of the DM profile for $S/N = 10$ in the case where the DM mini-spike harboring the IMBH has a radially power-law profile. The solid line, the dashed line, and the dashed-dotted line corresponds to $\Delta\alpha/\alpha$, $\Delta c_\epsilon/c_\epsilon$, $\Delta M_c/M_c$ respectively. For this plot, $\mu = 1M_\odot$ and the values of the parameters M_{BH} , ρ_{sp} , and r_{sp} are assumed as in the table I.

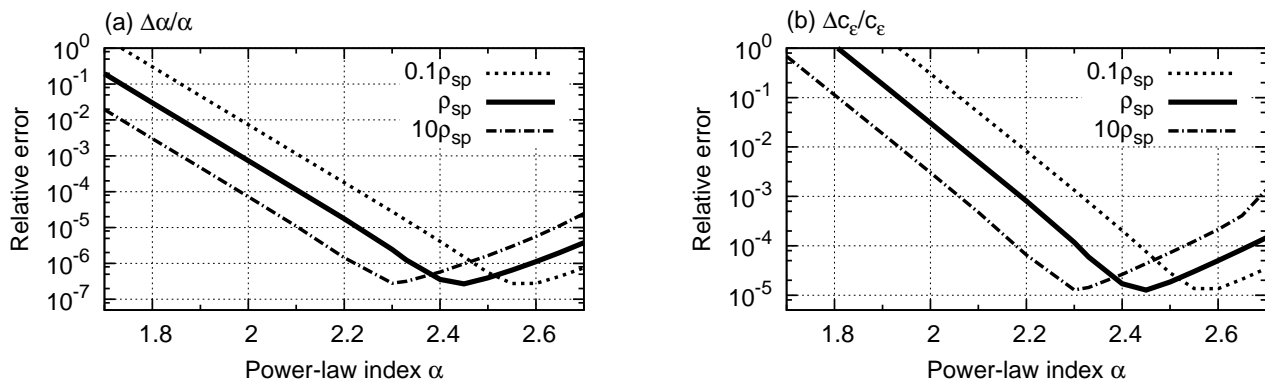


FIG. 6: The relative errors of (a) α and (b) c_ϵ versus the power-law index of the DM profile for $S/N = 10$ in the case where the DM mini-spike harboring the IMBH has a radially power-law profile. The solid line, the dashed line and the dashed-dotted line corresponds to ρ_{sp} , $0.1 \times \rho_{\text{sp}}$, and $10 \times \rho_{\text{sp}}$ respectively. The value of ρ_{sp} is taken from the table I.

surrounded by a DM mini-spike and a stellar mass compact object. The compact object falling into the central IMBH is affected by the gravitational interaction of both the IMBH and the DM mini-spike, namely the gravitational potential of both the IMBH and the DM mini-spike, gravitational wave back-reaction and dynamical friction. Then the resulting inspiral GW is modified by the DM mini-spike in comparison with the case where the IMBH has no DM mini-spike around it. Such a GW will be detected by future space-crafted detectors such as eLISA/NGO. We find that thanks to the DM parameters contained in the GW phase, the measurement errors of the DM parameters are very small for large power-law index of the mini-spike profile. To put it another way, we can extract the DM parameters very accurately from the GW waveform using matched filtering if the DM mini-spike has a steep profile. Indeed, in our reference case as originally advocated by [1, 2], we could determine the power-law index of the DM mini-spike radial profile with the 1σ relative error of $\pm 5 \times 10^{-6}$ for a GW signal with signal-to-noise-ratio 10 and assuming 5 years observation with eLISA, as shown in Fig. 3 and indicated by Eq. (41e). We also investigated how accurately the DM parameters can be determined for various DM parameters and the masses of the IMBH - stellar mass object binary surrounded by a DM mini-spike. We have found that smaller the mass of the stellar mass object, that of the IMBH, or the larger the power-law index of the DM mini-spike, we can measure DM parameters to better accuracy as shown in Figs. 4 and 5. Even a moderately flatter mini-spike with the radial distribution proportional to $r^{-1.7}$ would still allow us to determine the power-law index to 10 % accuracy.

Indirect dark matter searches in the gamma-ray band and through GW observation proposed in our previous [23] and current papers are complementary to each other. The GW observations we propose should be applicable to both very weakly annihilating and non-annihilating DM particles. Even if the DM particles do not weakly interact with each other, they affect the motion of the stellar mass object gravitationally and the resulting GW is modified by them. GW are insensitive to absorption and scattering in the interstellar medium during the propagation unlike electromagnetic waves. Therefore GW observations offer information on the DM mini-spike directly. On the other hand, if the DM particles self-annihilate, an annihilation plateau may develop within a

Hubble time [14] and the power-law index α of the DM radial profile becomes effectively zero within a radius r_{lim} . For the case of the values of the parameters listed in the table I, the DM mass 200GeV, and its cross section $\sigma v = 10^{-27} \text{cm}^3 \text{s}^{-1}$ [14], we find $r_{\text{lim}} \sim 2 \times 10^{-4} \text{pc}$ which is much larger than the initial orbital radius at which the GW frequency from the binary enters the eLISA detection frequency band. Hence in this case, gamma-ray searches are a better way to explore a DM mini-halo surrounding the IMBH, as indicated by Fig. 5.

In summary, the combination of gamma-ray observations with future GW observations will enable us to probe the structure of the DM mini-spike and even to offer hints that may clarify the nature of DM particles. Moreover, because the DM profile strongly depends on the formation history of the central IMBH, both types of observation may shed light on how the IMBH evolved with cosmic history.

Acknowledgments

The authors thank Jun'ichi Yokoyama and Enrico Barausse for useful comments. This work is supported by the Grant-in-Aid for JSPS Fellows No. 26-8636 (KE), the Grant-in-Aid for Young Scientists No. 25800126 (YI) and the MEXT Grant-in-Aid for Scientific Research on Innovative Areas ‘‘New Developments in Astrophysics Through Multi-Messenger Observations of Gravitational Wave Sources’’ (Grant Number 24103005) (YI).

Appendix A: Rewriting the GW waveform

Our goal in this appendix is to rewrite the waveform Eq. (25a) in the form of an explicit function of GW frequency f . According to Eqs. (25a), (25b) and (25c), the GW waveform from the binary system composed of the stellar mass object and the IMBH surrounded by DM mini-halo is expressed by

$$\tilde{h}(f) = \frac{1}{2} e^{i\Psi(t)} A(t) \left[\frac{2\pi}{\ddot{\Phi}(t)} \right]^{1/2}, \quad (\text{A1a})$$

$$\Psi(t) = 2\pi f \frac{D}{c} + \tilde{\Phi}(t) - \frac{\pi}{4}, \quad (\text{A1b})$$

$$\tilde{\Phi}(t) \equiv 2\pi f t - \Phi(t), \quad (\text{A1c})$$

where $A(t)$ is the time-dependent amplitude defined by Eq. (24b), $\Phi(t)$ is the time-dependent phase defined by Eq. (22c), and D is the distance to the source. We proceed as follows. We start with the amplitude $A/2\sqrt{2\pi/\ddot{\Phi}}$. The frequency f can be expressed in terms of the orbital radius R which is related to the time t by Eq. (19). So the amplitude can be expressed as a function of the frequency f through the relation between t and f . Next, we tackle the phase Ψ . Finally, combining these results, we find the explicit expression of the GW waveform in the Fourier domain.

1. Rewriting the amplitude

The GW frequency $f \equiv \omega_{\text{GW}}/2\pi$ which is defined by Eq. (11) is expanded in a Taylor series in a power of R :

$$\begin{aligned} f &= \frac{\omega_{\text{GW}}}{2\pi} \\ &= \frac{1}{\pi} \left[\frac{GM_{\text{eff}}}{R^3} + \frac{F}{R^\alpha} \right]^{1/2} \\ &= \frac{\sqrt{GM_{\text{eff}}}}{\pi} R^{-3/2} \left[1 + \frac{1}{2} R^{3-\alpha} \varepsilon - \frac{1}{8} R^{2(3-\alpha)} \varepsilon^2 + \dots \right]. \end{aligned} \quad (\text{A2})$$

Inverting this equation, we obtain R as a function of GW frequency and expanded in ε :

$$R = \delta^{1/(3-\alpha)} \left[1 + \frac{1}{3} \delta \varepsilon + \frac{2-\alpha}{9} \delta^2 \varepsilon^2 + \dots \right], \quad (\text{A3a})$$

$$\delta \equiv \left(\frac{GM_{\text{eff}}}{\pi^2 f^2} \right)^{(3-\alpha)/3}, \quad (\text{A3b})$$

where we introduce a new frequency variable δ defined by Eq. (A3b) for convenience. Using the definition of x given by Eq. (17), the dimensionless radius parameter x can be expanded in a power of ε :

$$x = (\delta \varepsilon)^{1/(3-\alpha)} \chi, \quad (\text{A4a})$$

$$\chi \equiv 1 + \frac{1}{3}\delta\varepsilon + \frac{2-\alpha}{9}\delta^2\varepsilon^2 + \dots, \quad (\text{A4b})$$

where we introduce χ for convenience. Note that the function χ is equal to one when a DM mini-spike is not present around an IMBH.

For later convenience, we rewrite dx/dt which is defined by Eq. (19) as follows.

$$\begin{aligned} \frac{dx}{dt} &= -c_{\text{GW}} \frac{(1+x^{3-\alpha})^3}{4x^3 [1+(4-\alpha)x^{3-\alpha}]} - c_{\text{DF}} \frac{1}{(1+x^{3-\alpha})^{1/2} [1+(4-\alpha)x^{3-\alpha}] x^{-5/2+\alpha}} \\ &= -c_{\text{GW}} f_{\text{GW}}(x) - c_{\text{DF}} f_{\text{DF}}(x) \\ &= -c_{\text{GW}} f_{\text{GW}}(x) \left[1 + \frac{c_{\text{DF}} f_{\text{DF}}(x)}{c_{\text{GW}} f_{\text{GW}}(x)} \right] \\ &= -c_{\text{GW}} f_{\text{GW}}(x) [1 + \tilde{c}J(x)], \end{aligned} \quad (\text{A5})$$

where functions $f_{\text{GW}}(x)$, $f_{\text{DF}}(x)$ and $J(x)$ and a coefficient \tilde{c} are defined by

$$f_{\text{GW}}(x) \equiv \frac{(1+x^{3-\alpha})^3}{4x^3 [1+(4-\alpha)x^{3-\alpha}]}, \quad (\text{A6a})$$

$$f_{\text{DF}}(x) \equiv \frac{1}{(1+x^{3-\alpha})^{1/2} [1+(4-\alpha)x^{3-\alpha}] x^{-5/2+\alpha}}, \quad (\text{A6b})$$

$$J(x) \equiv \frac{f_{\text{DF}}(x)}{f_{\text{GW}}(x)} = \frac{4x^{11/2-\alpha}}{(1+x^{3-\alpha})^{7/2}}, \quad (\text{A6c})$$

$$\tilde{c} \equiv \frac{c_{\text{DF}}}{c_{\text{GW}}}. \quad (\text{A6d})$$

The coefficient \tilde{c} is the ratio of the dynamical friction coefficient to the gravitational radiation coefficient. So \tilde{c} includes the DM information.

Next, we rewrite the second time derivative of Φ , $\ddot{\Phi}$, as a function of x . From Eq. (22c), $\ddot{\Phi}$ is expressed by

$$\begin{aligned} \ddot{\Phi}(t) &= \dot{\omega}_{\text{GW}} \\ &= -(GM_{\text{eff}})^{1/2} \varepsilon^{3/[2(3-\alpha)]} \frac{3 + \alpha x^{3-\alpha}}{x^{5/2} (1+x^{3-\alpha})^{1/2}} \frac{dx(t)}{dt}. \end{aligned} \quad (\text{A7})$$

To move from the first line to the second, we have made use of Eqs. (11) and (17). The time derivative of x displayed in the right-hand side of Eq. (A7) can be rewritten as a function of x by Eq. (A5). So we can express $\ddot{\Phi}$ as a function of x :

$$\begin{aligned} \ddot{\Phi}(t) &= (GM_{\text{eff}})^{1/2} \varepsilon^{3/[2(3-\alpha)]} c_{\text{GW}} [1 + \tilde{c}J(x)] \times f_{\text{GW}}(x) \frac{3 + \alpha x^{3-\alpha}}{x^{5/2} (1+x^{3-\alpha})^{1/2}} \\ &= (GM_{\text{eff}})^{1/2} \varepsilon^{3/[2(3-\alpha)]} c_{\text{GW}} [1 + \tilde{c}J(x)] \times \frac{3}{4} x^{-11/2} \frac{(1+x^{3-\alpha})^{5/2} (1 + \alpha x^{3-\alpha}/3)}{1 + (4-\alpha)x^{3-\alpha}} \\ &= (GM_{\text{eff}})^{1/2} \varepsilon^{3/[2(3-\alpha)]} c_{\text{GW}} [1 + \tilde{c}J(x)] \times \frac{3}{4} x^{-11/2} K(x), \end{aligned} \quad (\text{A8})$$

where the function $K(x)$ is defined by

$$K(x) \equiv \frac{(1+x^{3-\alpha})^{5/2} (1 + \alpha x^{3-\alpha}/3)}{1 + (4-\alpha)x^{3-\alpha}}. \quad (\text{A9})$$

Note that $K(x)$ is equal to one when a DM mini-spike is not present around an IMBH.

Substitution of Eqs. (11) and (17) into E. (24b) gives

$$A = \frac{4G\mu}{Dc^4} (\pi f)^2 \varepsilon^{-2/(3-\alpha)} x^2, \quad (\text{A10})$$

after some algebra and simplification. Combining Eqs. (A10) and (A8), we finally arrive at the final expression for the amplitude,

$$\frac{A}{2} \sqrt{\frac{2\pi}{\ddot{\Phi}}} = \frac{1}{2} \times \frac{4G\mu}{Dc^4} (\pi f)^2 \varepsilon^{2/(3-\alpha)} x^2 \times \sqrt{\frac{8\pi}{3}} (GM_{\text{eff}})^{-1/4} \varepsilon^{-3/[4(3-\alpha)]} c_{\text{GW}}^{-1/2} [1 + \tilde{c}J(x)]^{-1/2} x^{11/4} K(x)^{-1/2}$$

$$\begin{aligned}
&= \sqrt{\frac{32\pi^5}{3}} \frac{G\mu}{Dc^4} (GM_{\text{eff}})^{-1/4} c_{\text{GW}}^{-1/2} \varepsilon^{5/[4(3-\alpha)]} f^2 x^{19/4} [K(x)(1+\tilde{c}J(x))]^{-1/2} \\
&= \sqrt{\frac{5}{24}} \frac{1}{\pi^{2/3}} \frac{c}{D} \left(\frac{GM_c}{c^3}\right)^{5/6} f^{-7/6} \chi^{19/4} [K(x)(1+\tilde{c}J(x))]^{-1/2}, \tag{A11}
\end{aligned}$$

where M_c is defined by $M_c \equiv \mu^{3/5} M_{\text{eff}}^{5/2}$ and is called the chirp mass. From the second line to the third line, we have used Eqs. (18), (20a) and (A4a).

2. Rewriting the phase

Our next task is to express the phase Ψ given by Eq. (A1b) as a function of $x = x(f)$. From Eq. (A8), the time derivative of frequency df/dt is expressed by

$$\begin{aligned}
\frac{df}{dt} &= \frac{\ddot{\Phi}}{2\pi} \\
&= \frac{3}{8\pi} (GM_{\text{eff}})^{1/2} \varepsilon^{3/[2(3-\alpha)]} c_{\text{GW}} x^{-11/2} [K(1+\tilde{c}J)] \\
&= \frac{3}{5}\pi \left(\frac{8\pi GM_c}{c^3}\right)^{5/3} f^{11/3} \chi^{-11/2} [K(1+\tilde{c}J)]. \tag{A12}
\end{aligned}$$

We used Eqs. (20a) and (A4a) to go from the second line to the third line. Using Eq. (A12), we get

$$\Phi(f) = \frac{10}{3} \left(\frac{8\pi GM_c}{c^3}\right)^{-5/3} \int df' \frac{\chi^{11/2}}{f'^{8/3} K(1+\tilde{c}J)}, \tag{A13a}$$

$$2\pi ft = -\frac{10}{3} \left(\frac{8\pi GM_c}{c^3}\right)^{-5/3} f \int df' \frac{\chi^{11/2}}{f'^{11/3} K(1+\tilde{c}J)}, \tag{A13b}$$

where the constant of integration is determined by the initial condition of the GW phase.

3. Final form

Collecting the above results, Eqs. (A11), (A13a) and (A13b), we finally obtain the GW waveform in the frequency domain:

$$\tilde{h}(f) = \mathcal{A} f^{-7/6} e^{i\Psi(f)} \chi^{19/4} [K(x)(1+\tilde{c}J(x))]^{-1/2}, \tag{A14a}$$

$$\mathcal{A} = \left(\frac{5}{24}\right)^{1/2} \frac{1}{\pi^{2/3}} \frac{c}{D} \left(\frac{GM_c}{c^3}\right)^{5/6} \frac{1+\cos^2\iota}{2}, \tag{A14b}$$

$$\Psi(f) = 2\pi f \left(t_c + \frac{D}{c}\right) - \Phi_c - \frac{\pi}{4} - \tilde{\Phi}(f), \tag{A14c}$$

$$\tilde{\Phi}(f) = \frac{10}{3} \left(\frac{8\pi GM_c}{c^3}\right)^{-5/3} \left[-f \int_{\infty}^f df' \frac{\chi^{11/2}}{f'^{11/3} K(1+\tilde{c}J)} + \int_{\infty}^f df' \frac{\chi^{11/2}}{f'^{8/3} K(1+\tilde{c}J)} \right], \tag{A14d}$$

where \mathcal{A} is the overall amplitude, t_c is the coalescence time, Φ_c is the coalescence phase. Note that when a DM mini-spike is not present around an IMBH, $\chi \rightarrow 1$, $K \rightarrow 1$, $M_c \rightarrow M_{c0} \equiv \mu^{3/5} M_{\text{BH}}^{2/5}$, so the waveform becomes

$$\tilde{h}(f) = \mathcal{A} f^{-7/6} e^{i\Psi(f)}, \tag{A15a}$$

$$\mathcal{A} = \left(\frac{5}{24}\right)^{1/2} \frac{1}{\pi^{2/3}} \frac{c}{D} \left(\frac{GM_{c0}}{c^3}\right)^{5/6}, \tag{A15b}$$

$$\Psi(f) = 2\pi f \left(t_c + \frac{D}{c}\right) - \Phi_c - \frac{\pi}{4} - \tilde{\Phi}(f), \tag{A15c}$$

$$\tilde{\Phi}(f) = -\frac{3}{4} \left(\frac{GM_{c0}}{c^3} 8\pi f\right)^{-5/3}. \tag{A15d}$$

This is consistent with the waveform from the binary composed of two point-like compact object with mass μ and M_{BH} [43].

Appendix B: The number of GW cycles

The detector sensitivity to the inspiral GWs is closely related to the number of GW cycles. That is because N_{cycle} which is defined by Eq. (B1) is proportional to the GW phase which is defined by Eq. (22c). Therefore SNR strongly depends on the number of cycles N_{cycle} . The number of GW cycles in the frequency range $f \in [f_{\text{min}}, f_{\text{max}}]$ is defined by

$$N_{\text{cycle}} = \int_{t_{\text{min}}}^{t_{\text{max}}} dt \dot{f}(t) = \int_{f_{\text{min}}}^{f_{\text{max}}} df \frac{f}{\dot{f}}, \quad (\text{B1})$$

where an overdot denotes the time derivative and df/dt can be calculated by Eq. (39) (Note that $d\tau = -dt$).

We define the frequency bandwidth of eLISA as the frequency range $f \in [f_-, f_+]$ within which the square root of the noise spectral density is below half its minimum value:

$$\sqrt{S_n(f)} \leq 2\sqrt{S_n(f_{\text{best}})}, \quad (f \in [f_-, f_+]), \quad (\text{B2})$$

where f_{best} is the frequency at which the eLISA is most sensitive to the GWs. Because we assume 5 year observation, depending on the binary configuration, f_- may be smaller or larger than the initial frequency f_{ini} from which the inspiral GW frequency sweeps to the frequency at the innermost stable circular orbit, f_{ISCO} . Taking the initial frequency f_{ini} into account, the frequency bandwidth $[f_{\text{min}}, f_{\text{max}}]$ in which the inspiral GW sweeps is expressed by

$$f_{\text{min}} = \max\{f_{\text{ini}}, f_-\}, \quad (\text{B3a})$$

$$f_{\text{max}} = \min\{f_{\text{ISCO}}, f_+\}, \quad (\text{B3b})$$

and we obtain Fig. 7 from Eq. (B1). For $\alpha < 2.5$, the initial frequency f_{ini} at which the GW start to be observed is within the full width at half minimum of $\sqrt{S_n(f)}$. So the minimum frequency f_{min} which the inspiral GW spend in the detector bandwidth is equal to the initial frequency f_{ini} . On the other hand, for $\alpha > 2.5$, the initial frequency f_{ini} is out of the full width at half minimum. So f_{min} is equal to the lower bound of the detector bandwidth of eLISA f_- . Since f_+ is smaller than f_{ISCO} for all values of α and in the cases we studied, $f_{\text{max}} = f_+$

Using Eqs. (39), (B1), (B3a) and (B3b), the number of cycles N_{cycle} is obtained in Fig. 8. The figure shows that N_{cycle} is almost constant for small α but drops sharply for large α . This behavior of N_{cycle} is explained by the fact that the DM has more influence on the motion of the stellar mass object for larger α . For large α , df/dt increases sharply as $t \rightarrow t_c$ due to the DM effect and the GW frequency of the stellar mass object goes up rapidly through the frequency bandwidth of eLISA. It follows from this that larger α leads to wider frequency band but to the less number of GW cycles near the best sensitivity of the detector. The sensitivity to the GWs is determined by the competition between these two effects.

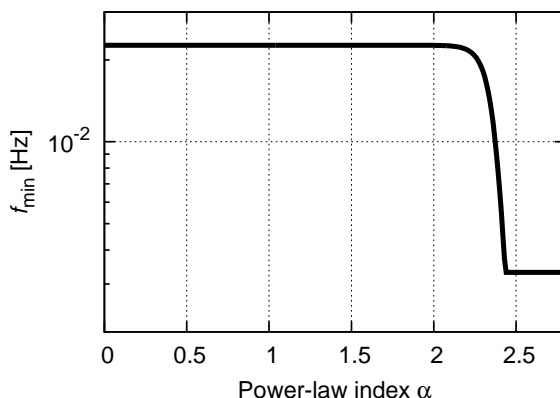


FIG. 7: Lower frequency bound which is the minimum frequency the inspiral GW spend in the detector bandwidth $[f_-, f_+]$ for $\mu = 1M_{\odot}$ and $M_{\text{BH}} = 10^3M_{\odot}$.

-
- [1] H.-S. Zhao and J. Silk, Phys. Rev. Lett. **95**, 011301 (2005), astro-ph/0501625.
 - [2] G. Bertone, A. R. Zentner, and J. Silk, Phys. Rev. D **72**, 103517 (2005), astro-ph/0509565.
 - [3] S. Arrenberg, H. Baer, V. Barger, L. Baudis, D. Bauer, J. Buckley, M. Cahill-Rowley, R. Cotta, A. Drlica-Wagner, J. L. Feng, et al., ArXiv e-prints (2013), 1310.8621.

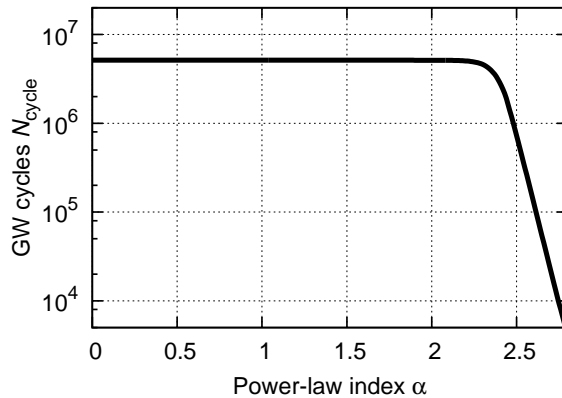


FIG. 8: The number of cycles N_{cycle} spent in the bandwidth $f \in [f_{\text{min}}, f_{\text{max}}]$ for $\mu = 1M_{\odot}$ and $M_{\text{BH}} = 10^3 M_{\odot}$. For large α , the number of cycles drops sharply because of the DM effect.

- [4] M. Ackermann, M. Ajello, A. Albert, A. Allafort, L. Baldini, G. Barbiellini, D. Bastieri, K. Bechtol, R. Bellazzini, E. Bissaldi, et al., *Phys. Rev. D* **88**, 082002 (2013).
- [5] J. Albert et al. (MAGIC Collaboration), *Astrophys. J.* **679**, 428 (2008), 0711.2574.
- [6] A. Abramowski, F. Acero, F. Aharonian, A. G. Akhperjanian, G. Anton, S. Balenderan, A. Balzer, A. Barnacka, Y. Becherini, J. Becker Tjus, et al., *Phys. Rev. Lett.* **110**, 041301 (2013), 1301.1173.
- [7] J. Grube and VERITAS Collaboration, in *American Institute of Physics Conference Series*, edited by F. A. Aharonian, W. Hofmann, and F. M. Rieger (2012), vol. 1505 of *American Institute of Physics Conference Series*, pp. 689–692, 1210.4961.
- [8] S. Funk, ArXiv e-prints (2013), 1310.2695.
- [9] P. Gondolo and J. Silk, *Phys. Rev. Lett.* **83**, 1719 (1999), astro-ph/9906391.
- [10] T. Nakano and J. Makino, *Astrophys. J. Lett.* **525**, L77 (1999), astro-ph/9906131.
- [11] P. Ullio, H. Zhao, and M. Kamionkowski, *Phys. Rev. D* **64**, 043504 (2001), astro-ph/0101481.
- [12] D. Merritt, M. Milosavljevic, L. Verde, and R. Jimenez, *Phys. Rev. Lett.* **88**, 191301 (2002), astro-ph/0201376.
- [13] D. Merritt, *Phys. Rev. Lett.* **92**, 201304 (2004), astro-ph/0311594.
- [14] G. Bertone and D. Merritt, *Phys. Rev. D* **72**, 103502 (2005), astro-ph/0501555.
- [15] X. Liu, Y. Shen, F. Bian, A. Loeb, and S. Tremaine, *Astrophys. J.* **789**, 140 (2014), 1312.6694.
- [16] E. Vasiliev, F. Antonini, and D. Merritt, *Astrophys. J.* **785**, 163 (2014), 1311.1167.
- [17] N. Webb, D. Cseh, E. Lenc, O. Godet, D. Barret, S. Corbel, S. Farrell, R. Fender, N. Gehrels, and I. Heywood, *Science* **337**, 554 (2012), 1311.6918.
- [18] R. R. Islam, J. E. Taylor, and J. Silk, *Mon. Not. R. Astron. Soc.* **340**, 647 (2003), astro-ph/0208189.
- [19] V. Rashkov and P. Madau, *Astrophys. J.* **780**, 187 (2014), 1303.3929.
- [20] P. Amaro-Seoane, J. R. Gair, M. Freitag, M. C. Miller, I. Mandel, C. J. Cutler, and S. Babak, *Classical and Quantum Gravity* **24**, 113 (2007), astro-ph/0703495.
- [21] P. Amaro-Seoane, S. Aoudia, S. Babak, P. Binetruy, E. Berti, et al., *GW Notes* **6**, 4 (2013), 1201.3621.
- [22] S. Kawamura, M. Ando, N. Seto, S. Sato, T. Nakamura, et al., *Classical Quant. Grav.* **28**, 094011 (2011).
- [23] K. Eda, Y. Itoh, S. Kuroyanagi, and J. Silk, *Phys. Rev. Lett.* **110**, 221101 (2013), 1301.5971.
- [24] C. F. Macedo, P. Pani, V. Cardoso, and L. C. Crispino, *Astrophys. J.* **774**, 48 (2013), 1302.2646.
- [25] E. Barausse, V. Cardoso, and P. Pani, ArXiv e-prints (2014), 1404.7140.
- [26] E. Barausse, V. Cardoso, and P. Pani, *Phys. Rev. D* **89**, 104059 (2014), 1404.7149.
- [27] J. F. Navarro, C. S. Frenk, and S. D. M. White, *Astrophys. J.* **490**, 493 (1997), arXiv:astro-ph/9611107.
- [28] T. Fukushima, A. Kawai, and J. Makino, *Astrophys. J.* **606**, 625 (2004), astro-ph/0306203.
- [29] N. Okabe and K. Umetsu, *Publ. Astron. Soc. Jpn* (2007), astro-ph/0702649.
- [30] M. Oguri, A. Taruya, and Y. Suto, *Astrophys. J.* **559**, 572 (2001), arXiv:astro-ph/0105248.
- [31] A. R. Duffy, J. Schaye, S. T. Kay, and C. Dalla Vecchia, *Mon. Not. R. Astron. Soc.* **390**, L64 (2008), 0804.2486.
- [32] G. D. Quinlan, L. Hernquist, and S. Sigurdsson, *Astrophys. J.* **440**, 554 (1995), astro-ph/9407005.
- [33] P. Young, *Astrophys. J.* **242**, 1232 (1980).
- [34] G. D. Quinlan, L. Hernquist, and S. Sigurdsson, *Astrophys. J.* **440**, 554 (1995), astro-ph/9407005.
- [35] L. Sadeghian, F. Ferrer, and C. M. Will, *Phys. Rev. D* **88**, 063522 (2013), 1305.2619.
- [36] R. Haas, R. V. Shcherbakov, T. Bode, and P. Laguna, *Astrophys. J.* **749**, 117 (2012), 1201.4389.
- [37] R. V. Shcherbakov, A. Pe'er, C. S. Reynolds, R. Haas, T. Bode, and P. Laguna, *Astrophys. J.* **769**, 85 (2013), 1212.4837.
- [38] M. MacLeod, J. Goldstein, E. Ramirez-Ruiz, J. Guillochon, and J. Samsing, ArXiv e-prints (2014), 1405.1426.
- [39] S. Chandrasekhar, *Astrophys. J.* **97**, 255 (1943).
- [40] J. Binney and S. Tremaine, *Galactic Dynamics: Second Edition* (Princeton University Press, 2008).
- [41] M. Maggiore, *Gravitational Waves: Volume 1: Theory and Experiments* (2007).
- [42] L. S. Finn, *Phys. Rev. D* **46**, 5236 (1992), gr-qc/9209010.
- [43] C. Cutler and E. E. Flanagan, *Phys. Rev. D* **49**, 2658 (1994), gr-qc/9402014.
- [44] P. Amaro-Seoane, S. Aoudia, S. Babak, P. Binetruy, E. Berti, et al., *Classical Quant. Grav.* **29**, 124016 (2012), 1202.0839.

- [45] C. Cutler, Phys. Rev. D **57**, 7089 (1998), gr-qc/9703068.
[46] In [23], we have used ρ_{NFW} instead of ρ_{DM} to estimate ρ_{sp} and r_{sp} .